

# Damba-ST: Domain-Adaptive Mamba for Efficient Urban Spatio-Temporal Prediction

Rui An<sup>†‡</sup>, Yifeng Zhang<sup>†</sup>, Ziran Liang<sup>†</sup>, Wenqi Fan<sup>†</sup>, Yuxuan Liang<sup>§</sup>, Xuequn Shang<sup>†\*</sup> Qing Li<sup>†\*</sup>

<sup>†</sup>Northwestern Polytechnical University, Xi'an, China

Email: rui77.an@connect.polyu.hk, shang@nwpu.edu.cn

<sup>‡</sup>The Hong Kong Polytechnic University, Hong Kong SAR

Email: {yifeng.zhang, ziran.liang}@connect.polyu.hk, wenqifan03@gmail.com, qing-prof.li@polyu.edu.hk

<sup>§</sup>The Hong Kong University of Science and Technology (Guangzhou), Guangzhou, China

Email: yuxliang@outlook.com

**Abstract**—Training urban spatio-temporal foundation models that generalize well across diverse regions and cities (i.e., cross-domain scenarios) is critical for deploying urban services in unseen or data-scarce regions. Recent studies have typically focused on fusing cross-domain spatio-temporal data to train unified Transformer-based models. However, these models suffer from quadratic computational complexity and high memory overhead, limiting their scalability and practical deployment. Inspired by the efficiency of Mamba, a state space model with linear time complexity, we explore its potential for efficient urban spatio-temporal prediction. However, directly applying vanilla Mamba as a spatio-temporal backbone leads to negative transfer and severe performance degradation in unseen regions. This is primarily due to inherent spatio-temporal heterogeneity and the recursive mechanism of Mamba’s hidden state updates, which limit cross-domain generalization. To overcome these challenges, we propose Damba-ST, a novel domain-adaptive Mamba-based model for efficient urban spatio-temporal prediction. Damba-ST retains Mamba’s linear complexity advantage while significantly enhancing its adaptability to heterogeneous domains. Specifically, we introduce two core innovations: (1) a domain-adaptive state space model that partitions the latent representation space into a shared subspace for learning cross-domain commonalities and independent, domain-specific subspaces for capturing intra-domain discriminative features; (2) three distinct Domain Adapters, which serve as domain-aware proxies to bridge disparate domain distributions and facilitate the alignment of cross-domain commonalities. Extensive experiments demonstrate the generalization and efficiency of Damba-ST. It achieves state-of-the-art performance on prediction tasks and demonstrates strong zero-shot generalization, enabling seamless deployment in new urban environments without extensive retraining or fine-tuning.

**Index Terms**—Spatio-Temporal Prediction, State Space Model (SSM), Mamba, Heterogeneous Data Management.

## I. INTRODUCTION

Traffic flows refer to the dynamic movement of various urban activities, such as human mobility and vehicle flow [1], [2]. These flows are characterized by both temporal and spatial dimensions, exhibiting variations in flow volumes at different intersections over time [3], [4]. Accurate spatio-temporal traffic prediction is crucial for optimizing urban infrastructure, alleviating potential congestion and delays, and enabling prompt responses to emergencies [5], [6], [7]. Despite

notable advancements in existing spatio-temporal modeling methods [8], [9], [10], [11], these models typically are designed for a specific domain, limiting their abilities to generalize to unfamiliar traffic environments effectively.

Over the past few years, pretrained foundation models have achieved significant success in Natural Language Processing (NLP) and Computer Vision (CV). These models, trained on open-domain datasets, excel at extracting and condensing knowledge across multiple domains, exhibiting strong generalization. Following this pathway, recent efforts have fused large-scale, cross-regional spatio-temporal data to develop a unified foundation model [12], [13]. However, these spatio-temporal foundation models face substantial challenges in computational demand and memory overhead, primarily arising from their reliance on “Transformer + X” architectures. Specifically, the core self-attention mechanism is utilized to capture temporal dynamics, while the “X” module—such as GNNs [13], [14], Graph Transformers, or spatial prompts [12]—is strategically used to model spatial dependencies. Therefore, given a spatio-temporal graph with  $N$  nodes over  $T$  time steps, the computational complexity of a fully self-attention model escalates to *unacceptable quadratic complexity* of  $\mathcal{O}(T^2)$  and  $\mathcal{O}(N^2)$ . As the scale of nodes and the length of time series increase, this complexity bottleneck in transformer-based architectures severely hinders scalability for large-scale traffic graphs and long-term traffic flow series, presenting significant challenges for implementation on edge and low-resource urban devices. Therefore, there is an urgent need to develop an efficient model to address the high computational complexities.

Recently, **Mamba** [15], [16], as a novel state space model (SSM), has gained increasing popularity for its efficient computational capabilities. Specifically, through introducing selective mechanisms and well-designed hardware-computational algorithms [16], Mamba delivers comparable modeling capabilities to Transformers while maintaining linear complexity with context length. Furthermore, Mamba-2 [17] extends these capabilities by proposing matrix multiplication based on the Structured State Space Duality (SSD) property, enabling the SSM backbone to perform parallel computations for greater efficiency. Given the advantages of (i) *high performance* facilitated by a selective mechanism, (ii) *rapid training and*

\*Corresponding authors.

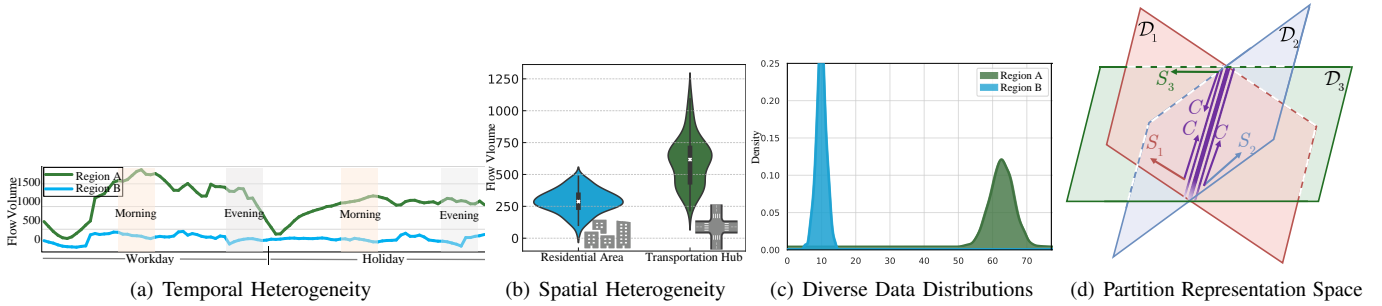


Fig. 1: **Spatio-Temporal Heterogeneity and Our Motivation.** (a) Regions A and B represent a transportation hub and residential area, each with distinct urban functions. Traffic patterns vary significantly over time (e.g., morning to evening and weekdays to holidays). (b) Distinct regions exhibit notable differences in traffic flow volume. (c) Such spatio-temporal heterogeneity leads to significant discrepancies in dataset distributions. (d) Given cross-domain data  $\{\mathcal{D}_1, \mathcal{D}_2, \mathcal{D}_3\}$ , we propose partitioning the Mamba representation space into a shared subspace for cross-domain commonalities, denoted as  $\mathcal{C}$ , and independent subspaces for domain-specific features, i.e.,  $\{\mathcal{S}_1, \mathcal{S}_2, \mathcal{S}_3\}$ .

*inference* through matrix multiplication and parallel processing, and (iii) *linear scalability* with context length, Mamba stands out as an efficient foundation model backbone in various tasks [16]. An increasing number of Mamba-based foundation models have been proposed, such as Jamba [18] in NLP, Vision Mamba [19], and VideoMamba [20] in CV, and Caduceus [21] in genomics.

Despite Mamba techniques have opened up opportunities to address the high computational complexity limitations of current Transformer-based foundation models, the development of Mamba-based spatio-temporal foundation models, specifically tailored for urban data, remains fully unexplored. Directly applying typical Mamba for cross-domain spatio-temporal data suffers from negative transfer and severe performance degradation in zero-shot predictions in unseen regions and cities. This limited generalization capability can be attributed to the following key factors: (1) **Spatio-temporal Heterogeneity**. Unlike language data, which typically share a common vocabulary, urban data lack explicit cross-domain invariants necessary for effective generalization due to inherent spatio-temporal heterogeneity, as illustrated in Fig. 1. Temporally, differences in traffic volumes, periods, trends, and timescales lead to inconsistent dynamics across domains. Spatially, variations in city layouts, road networks, and the distribution of transit hubs create further heterogeneity. Such spatio-temporal heterogeneity leads to significant discrepancies in cross-domain urban data distributions. (2) **Lack of Cross-Domain Adaptation**. The vanilla Mamba was originally designed for language sequences and lacks the necessary mechanisms to handle distributional discrepancies across domains, which are prevalent in urban data. As a result, it struggles to adapt to the heterogeneous patterns inherent in cross-domain urban scenarios. (3) **Recursive Drift Limits Generalization**. The recursive mechanism of hidden states  $h(t)$  and the state transition matrix  $\mathbf{A}$  in Mamba effectively captures and propagates past patterns. However, this recursive mechanism may lead to negative effects in the presence of data distribution change [22]. Specifically, when training on data from multiple domains, domain-specific features can be inadvertently accumulated or even amplified in the hidden states. This amplification may optimize performance

on seen domains but ultimately hinders the model’s ability to generalize to unseen domains.

Motivated by the above observations, we aim to address the inherent heterogeneity challenge and improve the generalization capability of the Mamba backbone through three key steps: (1) capturing domain-specific discriminative features, (2) identifying and aligning cross-domain commonalities, and (3) balancing the fine line between domain-specific discrimination and shared commonalities. Toward this goal, in contrast to existing urban foundation models that optimize a shared representation space through cross-domain data fusion training to fit all datasets, we propose to partition the Mamba representation space into two components, as illustrated in Figure 1(d): a shared subspace for learning cross-domain common patterns  $\mathcal{C}$ , and distinct, non-shared subspaces for domain-specific spatio-temporal patterns  $\{\mathcal{S}_1, \mathcal{S}_2, \mathcal{S}_3\}$ .

To this end, we propose a **Domain adaptive Mamba** for efficient urban Spatio-Temporal prediction, i.e., **Damba-ST**. It excels in strong generalizability across domains while maintaining the Mamba advantages of linear complexity. Damba-ST comprises three key modules: *Multi-View Encoding (MVE)*, *Intra-Domain Scanning (IDS)*, and *Cross-Domain Adaptation (CDA)*. Specifically, the MVE module decomposes the spatio-temporal data into three distinct views to effectively capture spatial, temporal, and spatio-temporal delay dependencies, and introduces “Domain-Adapters” that function as bridges to facilitate cross-domain pattern communication. The IDS module employs three scanning strategies to standardize the three perspectives’ data into a uniform sequence format. Then, these standardized sequences are fed into the CDA module to learn domain-adaptive representations. The CDA module is composed of three variants of the *Domain-Adaptive State Space Model (DASSM)*, each consisting of a Discrimination Learner, an Adapter Learner, and a Commonalities Learner. The Discrimination Learner captures domain-specific discriminative features, the Adapter Learner serves as a bridge to facilitate information exchange, and the Commonalities Learner identifies and aligns underlying patterns shared across domains. Finally, a fusion module combines features from three views and predicts future values. To sum up, our major contributions include:

- We introduce Damba-ST, a novel spatio-temporal prediction backbone with efficient linear computational complexity. To the best of our knowledge, Damba-ST is the first urban model designed to efficiently tackle the challenges of heterogeneity and quadratic computational complexity while exploring the generalizability of State Space Models in spatio-temporal contexts.
- We propose the Domain-Adaptive State Space Model, which addresses the heterogeneity challenge by partitioning the representation space into a shared subspace for learning cross-domain commonalities and independent subspaces for capturing domain-specific discriminative features. Additionally, we introduce the Domain Adapters that serve as domain-aware proxies to bridge disparate domain data and facilitate the alignment of cross-domain commonalities.
- Extensive experiments demonstrate the generalization and efficiency of Damba-ST. It achieves state-of-the-art performance on prediction tasks and demonstrates strong zero-shot generalization, enabling seamless deployment in new traffic environments without extensive retraining or fine-tuning.

## II. PRELIMINARIES

### A. Problem Formulation

1) **Urban Spatio-Temporal Data:** Urban flow is inherently spatio-temporal in nature, reflecting the spatial distribution and dynamic patterns of a city.

- The spatial component can be structured as a graph  $\mathcal{G} = (\mathcal{V}, \mathcal{E}, \mathcal{A})$ , where the node set  $\mathcal{V} = \{v_1, v_2, \dots, v_N\}$  represents the  $N$  sensors, the edges set  $\mathcal{E}$  defines the connectivity between the  $N$  sensors, and  $\mathcal{A} \in \mathbb{R}^{N \times N}$  is the weighted adjacency matrix, encoding spatial dependencies based on geographical distances.
- The temporal component  $\mathcal{X} = \{X_1, X_2, \dots, X_T\} \in \mathbb{R}^{T \times N}$  represents a multivariate time series over  $T$  time steps with  $N$  sensors. For convenience, we denote  $X_{:,n} \in \mathbb{R}^T$  as the  $n$ -th series over  $T$  time step.

2) **Spatio-Temporal Prediction and Generalization:** We adopt the end-to-end supervised training to predict the future  $F$  time steps of traffic metrics  $\mathcal{Y}^i \in \mathbb{R}^{F \times N}$  in city  $i$ . The pre-training dataset consists of  $M$  city spatio-temporal data, denoted as  $\mathbf{D}_{train} = \{(\mathcal{X}^i, \mathcal{G}^i, \mathcal{Y}^i) \mid i = 1, 2, \dots, M\}$ . Our objective is to train a generalized foundation model  $\mathcal{F}_\Theta(\cdot)$ , which is capable of capturing the underlying spatial, temporal, and spatio-temporal patterns that govern traffic dynamics across different spatial and temporal contexts. This model can be directly utilized to make predictions on unseen urban data  $\mathbf{D}_{unseen} = \{(\mathcal{X}^j, \mathcal{G}^j) \mid j > M\}$  without requiring extensive retraining or fine-tuning. The prediction and zero-shot generalization can be formally defined as:

$$\begin{aligned} \text{Training} : \mathcal{Y}^i &= \mathcal{F}_\Theta(\mathcal{X}^i, \mathcal{G}^i), \quad i \in \{1, 2, \dots, M\}, \\ \text{Generalization} : \mathcal{Y}^j &= \mathcal{F}_{\Theta_{frozen}}(\mathcal{X}^j, \mathcal{G}^j), \quad j > M. \end{aligned} \quad (1)$$

### B. Mamba

1) **State Space Model (SSM):** The classical State Space Models (SSMs) describes the state evolution of a linear time-invariant system, which map input signal  $\mathbf{x} = \{x(1), \dots, x(t), \dots\} \in \mathbb{R}^{L \times D} \mapsto \mathbf{y} = \{y(1), \dots, y(t), \dots\} \in \mathbb{R}^{L \times D}$  through implicit latent state  $h(t) \in \mathbb{R}^{N \times D}$ , where  $t, L, D$  and  $N$  indicate the time step, sequence length, channel number of the signal and state size, respectively. These models can be formulated as the following linear ordinary differential equations:

$$h'(t) = \mathbf{A}h(t) + \mathbf{B}x(t), \quad y(t) = \mathbf{C}h(t) + \mathbf{D}x(t), \quad (2)$$

where  $\mathbf{A} \in \mathbb{R}^{N \times N}$  is the state transition matrix that describes how states change over time,  $\mathbf{B} \in \mathbb{R}^{N \times D}$  is the input matrix that controls how inputs affect state changes,  $\mathbf{C} \in \mathbb{R}^{N \times D}$  denotes the output matrix that indicates how outputs are generated based on current states and  $\mathbf{D} \in \mathbb{R}^D$  represents the command coefficient that determines how inputs affect outputs directly. Most SSMs exclude the second term in the observation equation, i.e., set  $\mathbf{D}x(t) = 0$ , which can be recognized as a skip connection in deep learning models. The time-continuous nature poses challenges for integration into deep learning architectures. To alleviate this issue, most methods utilize the Zero-Order Hold rule [15] to discretize continuous time into  $K$  intervals, which assumes that the function value remains constant over the interval  $\Delta \in \mathbb{R}^D$ , the Eq. (2) can be reformulated as:

$$h_t = \bar{\mathbf{A}}h_{t-1} + \bar{\mathbf{B}}x_t, \quad y_t = \mathbf{C}h_t, \quad (3)$$

where  $\bar{\mathbf{A}} = \exp(\Delta \mathbf{A})$  and  $\bar{\mathbf{B}} = (\Delta \mathbf{A})^{-1}(\exp(\Delta \mathbf{A}) - \mathbf{I}) \cdot \Delta \mathbf{B}$ . Discrete SSMs can be interpreted as a combination of CNNs and RNNs. Commonly, the model uses the convolutional mode for efficient parallelizable training and switches into a recurrent mode for efficient autoregressive inference. The formulations in Eq. (3) are equivalent to the following convolution [23]:

$$\begin{aligned} \bar{\mathbf{K}} &= (\mathbf{C}\bar{\mathbf{B}}, \mathbf{C}\bar{\mathbf{A}}\bar{\mathbf{B}}, \dots, \mathbf{C}\bar{\mathbf{A}}^k\bar{\mathbf{B}}, \dots), \\ \mathbf{y} &= \mathbf{x} * \bar{\mathbf{K}}, \end{aligned} \quad (4)$$

Thus, the overall process can be represented as:

$$\mathbf{y} = \text{SSM}(\bar{\mathbf{A}}, \bar{\mathbf{B}}, \mathbf{C})(\mathbf{x}). \quad (5)$$

**Selective State Space Model (Mamba).** The discrete SSMs are based on data-independent parameters, meaning that parameters  $\bar{\mathbf{A}}$ ,  $\bar{\mathbf{B}}$ , and  $\mathbf{C}$  are time-invariant and the same for any input, limiting their effectiveness in compressing context into a smaller state [15]. Mamba [15] introduces a selective mechanism to filter out extraneous information while retaining pertinent details indefinitely. Specifically, it utilizes Linear Projection to parameterize the weight matrices  $\{\mathbf{B}_t\}_{t=1}^L$ ,  $\{\mathbf{C}_t\}_{t=1}^L$  and  $\{\Delta_t\}_{t=1}^L$  according to model input  $\{x_t\}_{t=1}^L$ , improving the context-aware ability, i.e.,:

$$\begin{aligned} \bar{\mathbf{B}}_t &= \text{Linear}_{\mathbf{B}}(x_t), \\ \bar{\mathbf{C}}_t &= \text{Linear}_{\mathbf{C}}(x_t), \\ \Delta_t &= \text{Softplus}(\text{Linear}_{\Delta}(x_t)). \end{aligned} \quad (6)$$

Then the output sequence  $\{y_t\}_{i=t}^L$  can be computed with those input-adaptive discretized parameters as follows:

$$h_t = \bar{\mathbf{A}}_t h_{t-1} + \bar{\mathbf{B}}_t x_t, \quad y_t = \bar{\mathbf{C}}_t h_t. \quad (7)$$

The selection mechanism hinders SSMs from supporting parallel training like CNNs. To overcome this, Mamba adopts Parallel Associative Scan [24] and Memory Recomputation. The former exploits linear associativity and the parallelism of GPUs and TPUs for memory-efficient computation, while the latter reduces memory usage by recomputing intermediate states during backpropagation.

### III. DAMBA-ST

In this section, we first introduce the novel concept of *Domain Adapters*, followed by a structural overview of the proposed Damba-ST. Subsequently, we present a detailed explanation of each model component.

#### A. Domain Adapters

Although spatio-temporal data lacks explicit cross-domain invariants for effective training and generalization, universal spatio-temporal principles are implicitly shared across diverse scenarios. For instance, while city layouts vary significantly, the relationships between different urban functional areas exhibit common structural patterns. Likewise, although temporal periodicity may differ across domains, it shares the fundamental rule of repetition.

To ensure that each domain retains its unique spatio-temporal characteristics while sharing these fundamental properties within a broader interconnected system, we introduce *Domain Adapters* tailored to each individual domain dataset. These adapters are randomly initialized as learnable embeddings that capture intra-domain underlying patterns. Furthermore, they are interconnected to serve as domain-specific proxies that communicate with one another, facilitating information exchange and bridging previously disconnected domain data. This mechanism is similar to the [CLS] token in ViT [25] and BERT, where a “blank slate” token as the sole input forces the model to encode a “general representation” of the entire sequence. Similar observations can be found in [26], [27], which demonstrate that the [CLS] token naturally absorbs domain-specific information, representing generalizable low-level information.

#### B. Structure Overview

As illustrated in Fig. 2, the proposed Damba-ST processes input cross-domain spatio-temporal data through three core modules: *Multi-View Encoding (MVE)*, *Intra-Domain Scanning (IDS)*, and *Cross-Domain Adaptation (CDA)*. The MVE module decomposes the spatio-temporal data into three distinct views to capture spatial, temporal, and spatio-temporal delay dependencies. The IDS module employs three scanning strategies to standardize the three views into a unified sequential format. These standardized sequences are then fed into the CDA module to learn domain-adaptive representations. Finally, a fusion module integrates features from the three views, and a linear

projection layer generates the traffic metric  $\mathcal{Y}$  for the next  $F$  time steps.

#### C. Multi-View Encoding (MVE)

To better understand the multifaceted factors influencing urban dynamic patterns, we decompose the spatio-temporal (ST) data into three views—Spatial, Temporal, and ST-delay—and introduce three distinct adapters to capture their respective dependencies. The encoding process for each view consists of two steps: intra-domain feature initialization and adapter initialization.

1) **Spatial View Encoding:** Traffic patterns vary across regions due to their unique geographical characteristics. For instance, sites with high connectivity typically experience higher traffic volumes. To capture the structural information of the traffic graph, we initialize node embeddings using topology-related features. Specifically, we compute the normalized Laplacian matrix of the traffic graph  $\mathcal{G}^i$ , defined as  $\Delta = \mathbf{I} - \mathbf{D}^{-1/2} \mathbf{A} \mathbf{D}^{-1/2}$ , where  $\mathbf{I}$  and  $\mathbf{D}$  denote the identity and degree matrices of  $\mathcal{G}^i$ , respectively. We then perform eigendecomposition of the Laplacian matrix, yielding  $\Delta = \mathbf{U} \Lambda \mathbf{U}^\top$ , where  $\mathbf{U}$  and  $\Lambda$  represent the eigenvector and eigenvalue matrices. The  $k$  smallest non-trivial eigenvectors are selected to form the initial node encodings, denoted as  $\Phi \in \mathbb{R}^{N \times k}$ . These encodings are subsequently projected through a linear layer to obtain the spatial representations  $\mathbf{S}^i = \{\mathbf{s}_1, \mathbf{s}_2, \dots, \mathbf{s}_N\} \in \mathbb{R}^{N \times D}$  for the  $N$  nodes in traffic graph  $\mathcal{G}^i$ .

The *spatio-adapter*  $\mathcal{S}^i$  of city  $i$  is a virtual node fully connected to all other nodes in the graph  $\mathcal{G}^i$ . It is initialized as a learnable embedding  $\mathcal{S}^i \in \mathbb{R}^D$ . This flexible design allows the spatio-adapter to iteratively refine its representation during training, enabling it to effectively capture intra-domain global spatial dependencies.

2) **Temporal View Encoding:** For the temporal component, we apply Reverse Instance Normalization [28] to each individual time series at every time step to alleviate temporal distribution shifts. Subsequently, to reduce time-step redundancy and extract local temporal semantics [29], we tokenize the normalized time series  $\mathcal{X}^i = \{X_1, X_2, \dots, X_T\} \in \mathbb{R}^{T \times N}$  into discrete patches using a 1D convolutional layer with output channel dimension  $D$ , kernel size  $P$ , and stride  $S$ . The number of patches is computed as  $L = \lfloor \frac{T-P}{S} \rfloor + 2$ , yielding the patch-level representation  $\mathbf{X}^i = \{\mathbf{x}_1, \mathbf{x}_2, \dots, \mathbf{x}_L\} \in \mathbb{R}^{L \times N \times D}$ , where the  $n$ -th time series is tokenized as  $X_{:,n} = \{x_{1,n}, x_{2,n}, \dots, x_{L,n}\} \in \mathbb{R}^{L \times D}$ .

The *temporal-adapter*  $\mathcal{T}^i \in \mathbb{R}^D$  for city  $i$  is a learnable patch embedding that captures intra-domain latent temporal transition dynamics through iterative updates during model training.

3) **ST-delay View Encoding:** There is a critical yet often underestimated dependency in urban modeling: spatio-temporal delay. In real-world traffic scenarios, delay propagation commonly exists among neighboring nodes. For instance, when a traffic incident occurs in a particular region, it may take several minutes to affect traffic conditions in adjacent areas.

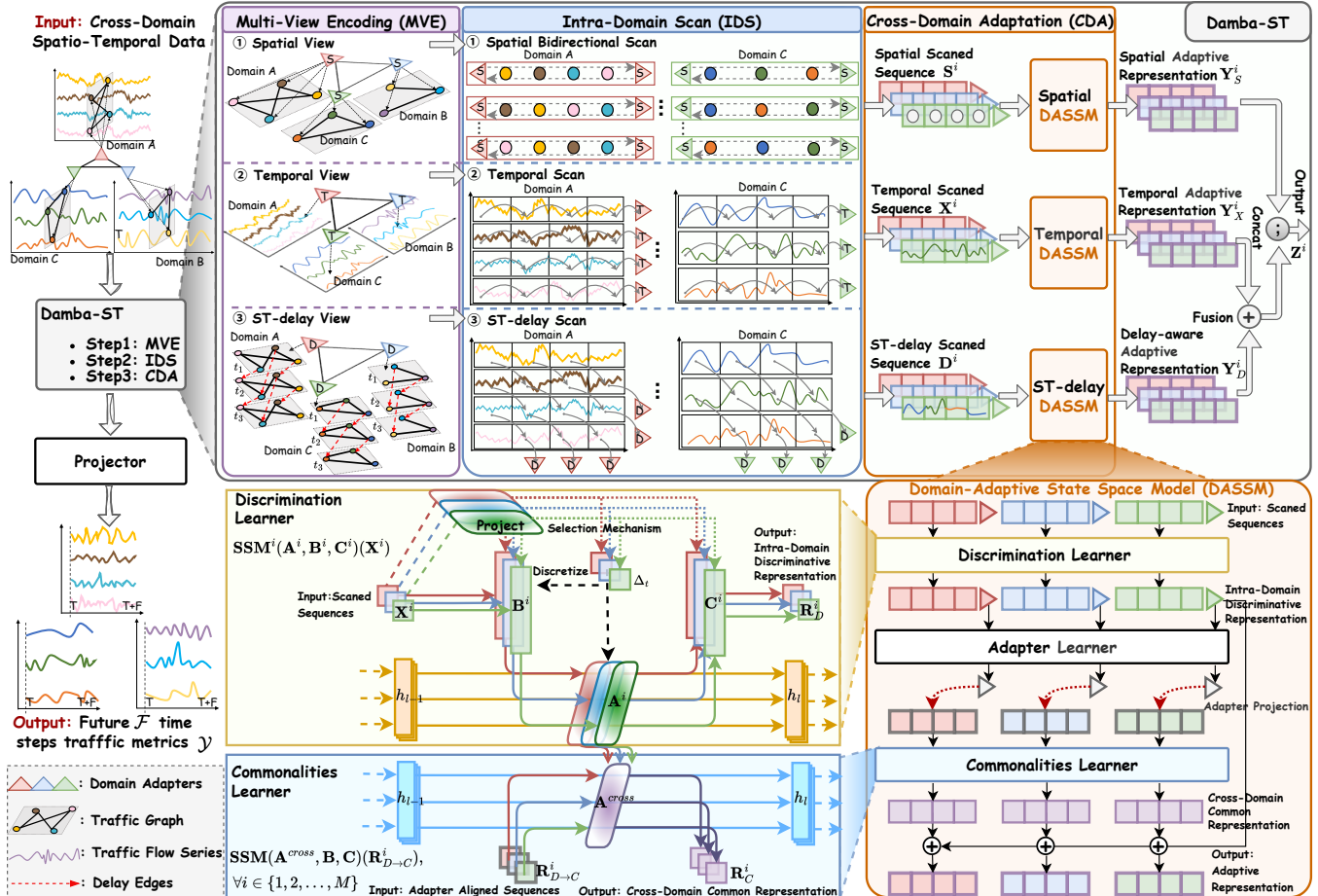


Fig. 2: **Overall framework.** Damba-ST comprises three key modules: *Multi-View Encoding (MVE)*, *Intra-Domain Scanning (IDS)*, and *Cross-Domain Adaptation (CDA)*. The CDA module further integrates three variants of the *Domain-Adaptive State Space Model (DASSM)*: *Spatial DASSM*, *Temporal DASSM*, and *ST-Delay DASSM*. Each variant contains a *Discrimination Learner*, an *Adapter Learner*, and a *Commonalities Learner*.

However, this delay effect is largely overlooked in existing traffic forecasting models. To accurately capture propagation delay, we propose a two-step strategy. Specifically, for each connected node pair  $(v_a, v_b)$ , the propagation delay  $\tau_{ab}$  is estimated by maximizing the cross-correlation [30] between their respective time series  $X_{:,a} \in \mathbb{R}^T$  and  $X_{:,b} \in \mathbb{R}^T$  via temporal shifting [31], formulated as:

$$\tau_{ab} = \arg \max_t \text{corr}(X_{:,a} \xrightarrow{t} X_{:,b}), \quad (8)$$

where  $\xrightarrow{t}$  denotes a  $t$ -step shift applied to  $X_{:,a}$ , and  $\text{corr}$  represents the Pearson correlation function. We estimate the delay values for all connected node pairs in advance and obtain the delay propagation adjacency matrix  $\tau \in \mathbb{R}^{N \times N}$ , which encodes the delay value between connected node pairs. Additionally, since traffic delays are dynamically influenced by temporal factors—such as longer delays during commuting hours—we introduce a timestamp-aware feature  $\tau(t) = \text{MLP}(t)$  to adjust the base delays dynamically. Here, the timestamp feature is defined as  $t = \{t^d; t^w\} \in \mathbb{R}^{T \times 2}$ , where  $t^d \in \mathbb{R}^T$  represents the time of day and  $t^w \in \mathbb{R}^T$  denotes the day of the week.

The final delay matrix is computed as  $\tau = \tau + \tau(t)$ , which serves as an indicator for scanning relevant historical temporal patches from neighboring nodes in the Section III-D3.

The *ST-delay adapter*  $\mathcal{D}^i$  for city  $i$  is prepended with a learnable embedding designed to capture latent delay dependencies.

#### D. Intra-Domain Scanning (IDS)

In this subsection, we introduce three scanning strategies to standardize the three views of the *MVE* module into a uniform sequential format for subsequent learning.

1) **Spatial Bidirectional Scan:** Given that topological nodes do not have a specific order, we employ a bidirectional scan to transform the spatial structure into a uniform sequential format. Specifically, we perform random walks on the traffic graph to generate  $N$  paths, each starting from a distinct node  $v_a$  with length  $L - 2$ , such as  $\text{path}_{v_a} = (v_a \rightarrow v_b \rightarrow \dots \rightarrow v_g)$ . To enable the *spatio-adapter*  $\mathcal{S}^i$  to capture global spatial dependencies, we attach it to both the beginning and the end of each path. Since spatial nodes are unordered, we scan each path in both forward and backward directions to eliminate

sequential order bias. For example, the standardized spatial sequences of path<sub>v<sub>a</sub></sub> are:

$$\begin{aligned}\vec{\mathbf{S}}_{v_a} &= \{\mathcal{S}^i; \mathbf{s}_a, \mathbf{s}_b, \dots, \mathbf{s}_g; \mathcal{S}^i\} \in \mathbb{R}^{L \times D}, \\ \overleftarrow{\mathbf{S}}_{v_a} &= \{\mathcal{S}^i; \mathbf{s}_g, \dots, \mathbf{s}_b, \mathbf{s}_a; \mathcal{S}^i\} \in \mathbb{R}^{L \times D}.\end{aligned}\quad (9)$$

Then, the standardized spatial sequence for all  $N$  paths in city  $i$  are expressed as:

$$\mathbf{S}^i = \{\overleftarrow{\mathbf{S}}_{v_1}, \overleftarrow{\mathbf{S}}_{v_2}, \dots, \overleftarrow{\mathbf{S}}_{v_N}\} \in \mathbb{R}^{N \times L \times D}, \quad (10)$$

where  $\overleftarrow{\mathbf{S}}_{v_n}$  represent the bidirectional spatial sequence of path<sub>v<sub>n</sub></sub>.

2) **Temporal Scan**: The time series patches naturally follow chronological order. To enable the *temporal-adapter*  $\mathcal{T}^i$  to learn underlying temporal state transition patterns, we append  $\mathcal{T}^i$  to the end of each series of patches. The standardized temporal sequence series in domain  $i$  is:

$$\mathbf{X}^i = \{\mathbf{x}_1, \mathbf{x}_2, \dots, \mathbf{x}_L; \mathcal{T}^i\} \in \mathbb{R}^{(L+1) \times N \times D} \quad (11)$$

3) **ST-delay Scan**: Spatio-temporal delay dependencies propagate along delay edges between graph snapshots. To standardize the ST-delay view into a uniform delay propagation sequence, we connect temporal patches based on the delay matrix  $\tau$ . Specifically, for a connected node path path<sub>v<sub>a</sub></sub> = ( $v_a \rightarrow v_b \rightarrow v_c$ ), a standardized ST-delay propagation sequence begins with the  $l$ -th temporal patch  $x_{l,a}$  of node  $v_a$ . According to the delay value  $\tau_{ab}$ , this temporal patch is propagated to the temporal patch  $x_{l+\lfloor \frac{\tau_{ab}}{P} \rfloor, b}$  on node  $v_b$  after  $\lfloor \frac{\tau_{ab}}{P} \rfloor$  time steps, where  $P$  denotes the patch length. Similarly, the propagation continues to node  $v_c$  after an additional  $\lfloor \frac{\tau_{bc}}{P} \rfloor$  time steps. To capture the latent delay dependencies in each specific city, we append the *ST-delay adapter*  $\mathcal{D}^i$  to the end of each scanned delay propagation sequence. Thus, a complete delay propagation sequence along the node path path<sub>v<sub>a</sub></sub> = ( $v_a \rightarrow v_b \rightarrow v_c$ ) can be expressed as:

$$\mathbf{D}_{v_a} = \{x_{l,a}, x_{l+\lfloor \frac{\tau_{ab}}{P} \rfloor, b}, x_{l+\lfloor \frac{\tau_{ab}}{P} \rfloor + \lfloor \frac{\tau_{bc}}{P} \rfloor, c}; \mathcal{D}^i\}. \quad (12)$$

We fix the number of patches in each delay path to  $L$ , then, the standardized delay propagation sequence for all  $N$  paths in domain  $i$  are expressed as:

$$\mathbf{D}^i = \{\mathbf{D}_{v_1}, \mathbf{D}_{v_2}, \dots, \mathbf{D}_{v_N}\} \in \mathbb{R}^{N \times L \times D}. \quad (13)$$

### E. Cross-Domain Adaptation (CDA)

The CDA module integrates three variants of the *Domain-Adaptive State Space Model (DASSM)*: Spatial DASSM, Temporal DASSM, and ST-delay DASSM, each designed to learn domain-adaptive representations.

In the remainder of this section, we use the temporal scanned sequences  $\mathbf{X}^i$  as an illustrative example to detail the design of the proposed DASSM. As shown in Fig. 2, DASSM comprises three primary components: 1) the *Discrimination Learner*, which captures domain-specific patterns through intra-domain optimization; 2) the *Adapter Learner*, which enables cross-domain generalization via adapter communication; and 3) the *Commonalities Learner*, which extracts shared patterns through cross-domain fusion optimization.

1) **Discrimination Learner**: In contrast to existing foundation models that fuse cross-domain data to learn a shared representation space, we propose the Discrimination Learner, which optimizes independent, domain-specific subspaces for each domain. This design enables the model to fully exploit domain-specific patterns induced by inherent heterogeneity. Given the standardized temporal sequence  $\mathbf{X}^i = \{\mathbf{x}_1, \mathbf{x}_2, \dots, \mathbf{x}_L; \mathcal{T}^i\} \in \mathbb{R}^{(L+1) \times N \times D}$  from Eq. (11), where  $i \in \{1, 2, \dots, M\}$  is the domain index, the Discrimination Learner trains a selective state space model  $\mathbf{SSM}^i$  for each domain  $i$  to capture intra-domain token dependencies. This process can be formulated as:

$$\mathbf{R}_D^i = \mathbf{SSM}^i(\mathbf{A}^i, \mathbf{B}^i, \mathbf{C}^i)(\mathbf{X}^i), \quad (14)$$

where  $\mathbf{R}_D^i \in \mathbb{R}^{(L+1) \times N \times D}$  is discriminative representation of sequence  $\mathbf{X}^i$ .

The domain-adapter  $\mathcal{T}^i \in \mathbb{R}^D$  is appended as the final token in the sequence and possesses a global receptive field, enabling it to effectively capture and aggregate global dependency information. Its learnable embedding is continuously refined during training. The computation process is defined as follows:

$$\begin{aligned}\mathbf{h}_{L+1}^i &= \mathbf{A}_{L+1}^i \mathbf{h}_L + \mathbf{B}_{L+1}^i \mathcal{T}^i, \\ \mathcal{T}^i &= \mathbf{C}_{L+1}^i \mathbf{h}_{L+1}^i.\end{aligned}\quad (15)$$

2) **Adapter Learner**: Similar to the `[CLS]` token in ViT [25], the domain-adapter  $\mathcal{T}^i$  serves as a proxy of intra-domain latent patterns. To facilitate cross-domain knowledge transfer, we introduce the Adapter Learner, which enables communication among domain adapters and promotes high-level knowledge sharing cross-domain. Specifically, the domain-adapters from all  $M$  domains are concatenated to form an adapter sequence  $\mathcal{T} = \{\mathcal{T}^1, \mathcal{T}^2, \dots, \mathcal{T}^M\} \in \mathbb{R}^{M \times D}$ . We then randomly shuffle the sequence order and apply both forward and backward SSM to ensure efficient bidirectional information exchange among adapters. This process can be formulated as:

$$\hat{\mathcal{T}} = \vec{\mathbf{SSM}}(\mathbf{A}, \mathbf{B}, \mathbf{C})(\mathcal{T}) + \overleftarrow{\mathbf{SSM}}(\mathbf{A}, \mathbf{B}, \mathbf{C})(\mathcal{T}), \quad (16)$$

where  $\hat{\mathcal{T}} = \{\hat{\mathcal{T}}^1, \hat{\mathcal{T}}^2, \dots, \hat{\mathcal{T}}^M\} \in \mathbb{R}^{M \times D}$  denotes the set of domain-adapters after exchanging information within a larger, interconnected system through adapter communication. Thus,  $\hat{\mathcal{T}}$  can be interpreted as the common pattern shared cross-domains.

3) **Commonalities Learner**: To optimize the shared representation subspace, we propose the Commonalities Learner, which harmonizes heterogeneous domain data and aligns cross-domain commonalities through intra-domain feature projection and cross-domain fusion optimization. Specifically, we first mitigate cross-domain heterogeneity by projecting the intra-domain discriminative representation  $\mathbf{R}_D^i$  onto their corresponding domain-adapter  $\hat{\mathcal{T}}^i$ . This projection is defined as:

$$\mathbf{R}_{D \rightarrow C}^i = \text{proj}(\mathbf{R}_D^i, \hat{\mathcal{T}}^i) = \left( \frac{\mathbf{R}_D^i \hat{\mathcal{T}}^{i \top}}{\|\hat{\mathcal{T}}^i\|^2} \right) \hat{\mathcal{T}}^i. \quad (17)$$

This projection operation can be seen as transforming the original domain-specific heterogeneous features to align with

the cross-domain commonalities captured by  $\hat{\mathcal{T}}^i$  (see Section III-G2 for theoretical justification). Then, we optimize the shared subspace by cross-domain fusion training, formulated as:

$$\mathbf{R}_C^i = \text{SSM}(\mathbf{A}^{\text{cross}}, \mathbf{B}, \mathbf{C})(\mathbf{R}_{D \rightarrow C}^i), \quad \forall i \in \{1, 2, \dots, M\}, \quad (18)$$

where the shared state transition matrix  $\mathbf{A}^{\text{cross}}$  is initialized as the mean of the matrices  $\mathbf{A}^i$  learned by the  $M$  Discrimination Learners, i.e.,  $\mathbf{A}^{\text{cross}} = \frac{1}{M} \sum_{i=1}^M \mathbf{A}^i$ . The resulting  $\mathbf{R}_C^i \in \mathbb{R}^{L \times N \times D}$  represents the cross-domain common representation.

Finally, we fuse the Discriminative Representation  $\mathbf{R}_D^i$  and the Common Representation  $\mathbf{R}_C^i$  using a fusion layer to obtain the final domain-adaptive representation  $\mathbf{Y}^i$  for domain  $i$ , defined as:

$$\mathbf{Y}^i = w_1 \cdot \text{Linear}(\mathbf{R}_D^i) + w_2 \cdot \text{Linear}(\mathbf{R}_C^i), \quad (19)$$

where  $w_1$  and  $w_2$  are hyperparameters that control the relative contributions of the discriminative and common components. The overall process of DASSM can be represented as:

$$\mathbf{Y}^i = \text{DASSM}(\mathbf{X}^i), \quad \forall i \in \{1, 2, \dots, M\}. \quad (20)$$

4) **DASSM Variants:** We adopt DASSM in three specialized variants: DASSM<sub>S</sub>, DASSM<sub>T</sub>, and DASSM<sub>D</sub>. Specifically, DASSM<sub>S</sub> captures the spatial adaptive representation  $\mathbf{Y}_S^i$  from the spatial scanned sequences  $\mathbf{S}^i$ , DASSM<sub>T</sub> learns the temporal adaptive representation  $\mathbf{Y}_X^i$  from the temporal scanned sequences  $\mathbf{X}^i$ , and DASSM<sub>D</sub> extracts the delay-aware adaptive representation  $\mathbf{Y}_D^i$  from the ST-delay scanned sequences  $\mathbf{D}^i$ , formulated as:

$$\begin{aligned} \mathbf{Y}_S^i &= \text{DASSM}_S(\mathbf{S}^i), \\ \mathbf{Y}_X^i &= \text{DASSM}_T(\mathbf{X}^i), \\ \mathbf{Y}_D^i &= \text{DASSM}_D(\mathbf{D}^i), \quad \forall i \in \{1, 2, \dots, M\}. \end{aligned} \quad (21)$$

Finally, we fuse the domain-adaptive representation features from the three models. First, we integrate the temporal adaptive representation  $\mathbf{Y}_X^i$  with the delay-aware representation  $\mathbf{Y}_D^i$  to form the temporal component, as both capture temporal patterns—encoding self-dynamics and interaction dynamics of the time series, respectively. We then concatenate this temporal component with the spatial adaptive representation  $\mathbf{Y}_S^i$  to construct the final spatio-temporal adaptive representation  $\mathbf{Z}^i$ , defined as:

$$\mathbf{Z}^i = ((\mathbf{Y}_X^i \oplus \mathbf{Y}_D^i); \mathbf{Y}_S^i). \quad (22)$$

After obtaining the final representation from Damba-ST, we apply a linear projection layer to generate the predicted traffic metric  $\mathcal{Y}_{\text{pred}}^i \in \mathbb{R}^{F \times N}$  for the next  $F$  time steps.

#### F. Model Optimization

We adopt the end-to-end supervised training to predict the future  $F$  time steps of traffic metrics. The objective function can be formulated as:

$$\begin{aligned} &\arg \min_{\Theta} \sum_{i=1}^M \mathcal{L}_{\Theta}^i, \\ &\text{s.t. } \mathcal{L}_{\Theta}^i = |(\mathcal{Y}^i, \mathcal{F}_{\Theta}(\mathcal{X}^i, \mathcal{G}^i))|, \end{aligned} \quad (23)$$

where  $\Theta$  represents all the learnable parameters in the network,  $\mathcal{Y}^i$  is the ground truth. We choose L1 loss as our training objective. Additionally, to enlarge the separation between Discrimination Learner and Commonalities Learner, we introduce two regularization terms in our objective function, i.e., *Model Differences* and *Representation Differences* [32], [33].

The *Model Differences* regularization terms  $S_m(\theta_D, \theta_C)$  constrain the parameter similarity between the Discrimination Learner  $\theta_D$  and Commonalities Learner  $\theta_C$ , which can prevent overfitting and improve generalization. We use the well-known exponential kernel to measure the parameter similarity, expressed as:

$$S_m(\theta_D, \theta_C) = \exp \left( -\frac{\|\theta_D - \theta_C\|_F}{2\sigma^2} \right), \quad (24)$$

where  $\|\theta_D - \theta_C\|_F$  is the Frobenius norm, measuring the parameter distance,  $\sigma$  is a regularization parameter that controls the range of similarity, and  $\exp(\cdot)$  is the exponential function.

The *Representation Differences* regularization terms  $S_r(\theta_D, \theta_C)$  constraints the overlap between discriminative representations  $\mathbf{R}_D$  and Common representations  $\mathbf{R}_C$ . The distance function is defined as:

$$S_r(\mathbf{R}_D, \mathbf{R}_C) = \frac{1}{C_0} \|\mathbf{R}_D^T \cdot \mathbf{R}_C\|, \quad (25)$$

where  $C_0 > 0$  is a normalization parameter. The final objective function of Urban-SSM is then achieved by combining Eq. (23) with (24) and (25), i.e.,

$$\arg \min_{\Theta} \sum_{i=1}^M \mathcal{L}_{\Theta}^i + \alpha S_m(\theta_D, \theta_C) + \beta S_r(\mathbf{R}_D, \mathbf{R}_C), \quad (26)$$

where  $\alpha$  and  $\beta$  are two balance parameters. The overall algorithm is presented in Algorithm 1.

#### G. DASSM Discussion

In this section, we further interpret how domain adapters facilitate cross-domain knowledge transfer in a two-fold manner and provide a theoretical analysis.

1) *Domain Adapters function as Intra-Domain Proxies*: The three domain adapters are randomly initialized as learnable embeddings and appended to the end of each sequence to ensure a global receptive field. The update mechanism consists of two stages:

- **Intra-Domain Update**: During intra-domain training within the Discrimination Learner, each domain adapter aggregates information from all other tokens in the same domain (global feature aggregation), with the computation process defined in Eq. (15). In this phase, the SGD backpropagation pushes the Discrimination Learner to encode intra-domain global patterns into the learnable embedding.
- **Cross-Domain Update**: During cross-domain training within the Adapter Learner, the domain adapters from all  $M$  domains are concatenated to form an adapter sequence, as defined in Eq. (16). Backpropagation then pushes information exchange among adapters, allowing each to encode cross-domain generalizable patterns into its learnable embedding.

---

**Algorithm 1:** Damba-ST

**Input:** Cross-domain urban data  $\mathbf{D}_{train} = (\mathcal{X}^i, \mathcal{G}^i)$ ,  $i \in \{1, 2, \dots, M\}$ , Number of training epochs  $T$ , learning rate  $\eta$ , hyper-parameters  $w_1, w_2, \alpha, \beta$ .

**Output:** Future  $F$  time steps traffic metrics  $\mathcal{Y}_{pred}^i$ .

/\* Training Stage \*/

- 1 Randomly initialize model  $\mathcal{F}_\Theta(\cdot)$  parameter  $\Theta$ , spatial-adapter embedding  $\mathcal{S}^i$ , temporal-adapter  $\mathcal{T}^i$  and spatio-temporal delay adapter  $\mathcal{D}^i$ ,  $\forall i \in \{1, 2, \dots, M\}$ <sup>1</sup>
- 2 **for**  $t = 1, 2, \dots, T$  **do**
- 3     Calculate spatial view encoding  $\mathbf{S}$ , temporal view encoding  $\mathbf{X}$  and delay value  $\tau$ ;
- 4     Scan spatial sequence  $\mathbf{S}$ , temporal sequence  $\mathbf{X}$  and delay propagation sequence  $\mathbf{D}$  via Eq. (10), (11), and (13);
- 5     **for** DASSM variants in  $\{\text{DASSM}_S, \text{DASSM}_T, \text{DASSM}_D\}$  in parallel **do**
- 6         Calculate intra-domain discriminative representation  $\mathbf{R}_D$  via Eq. (14);
- 7         Project intra-domain discriminative representation  $\mathbf{R}_D$  to domain-adapter via Eq. (17);
- 8         Calculate cross-domain common representation  $\mathbf{R}_C$  via Eq. (18);
- 9         Calculate domain-adaptive representation  $\mathbf{Y}$  via Eq. (19);
- 10     **end**
- 11     Fuse spatio-temporal representation  $\mathbf{Z}$  via Eq. (22);
- 12      $\mathcal{Y}_{pred} = \text{Proj}(\mathbf{Z})$ ;
- 13     Compute the loss objective via Eq. (26);
- 14      $\Theta \leftarrow \Theta - \eta \nabla_\Theta \mathcal{L}$ ;
- 15 **end**
- 16 **return** a generalized spatial-temporal foundation model  $\mathcal{F}_\Theta(\cdot)$ .
- /\* Zero-shot Generalization Stage \*/
- 17 **for** unseen urban data  $\mathbf{D}_{unseen} = \{(\mathcal{X}^j, \mathcal{G}^j) \mid j > M\}$  **do**
- 18      $\mathcal{Y}^j = \mathcal{F}_{\Theta_{frozen}}(\mathcal{X}^j, \mathcal{G}^j)$ .
- 19 **end**

---

2) *The Commonalities Learner Learns a Transformation from Domain-Specific Discriminative Patterns to Generalized Common Patterns:* It is worth noting that our proposed Commonalities Learner has the same theory support as Graph Prompt [34], [35], which has been proven equivalent to any form of prompting function for achieving universal graph transformations. We extend this idea to the spatio-temporal scenario, enabling the Commonalities Learner to theoretically achieve an effect equivalent to any form of spatio-temporal prompting function. This allows it to transform domain-specific discriminative patterns into generalized common patterns.

<sup>1</sup>For simplicity, we omit the superscript domain index  $i$  in the following notation to represent data from all  $M$  domains.

Specifically, since the domain adapter is a learnable embedding, the projection operation  $\text{proj}(\mathbf{R}_D^i, \hat{\mathcal{T}}^i)$  in Eq. (17) is equivalent to adding a learnable prompt  $P$  to the original features  $\mathbf{R}_D^i$ , resulting the prompted features  $\mathbf{R}_{D \rightarrow C}^i$ , formulated as:

$$\begin{aligned} \mathbf{R}_{D \rightarrow C}^i &= \left( \frac{\mathbf{R}_D^i \hat{\mathcal{T}}^{i\top}}{\|\hat{\mathcal{T}}^i\|^2} \right) \hat{\mathcal{T}}^i \\ &= \mathbf{R}_D^i + \left( \frac{\mathbf{R}_D^i \hat{\mathcal{T}}^{i\top}}{\|\hat{\mathcal{T}}^i\|^2} \hat{\mathcal{T}}^i - \mathbf{R}_D^i \right) \\ &= \mathbf{R}_D^i + P, \end{aligned} \quad (27)$$

where the orthogonal residual serves as the learnable prompt  $P$ . The Commonalities Learner is trained on these prompted features to optimize the shared representation subspace. This mechanism is theoretically equivalent to any domain-generalized transformation, thereby facilitating generalization across domains. Without loss of generality, we symbolize this projection operation as:

$$\hat{\mathcal{X}} = \mathcal{X} + P \quad (28)$$

**Theorem 1.** *(Generalization Capability of Learnable Prompt  $P$ ) Given a Spatio-Temporal model  $\mathcal{F}_\Theta$ , and the input spatio-temporal data  $(\mathcal{G}, \mathcal{X})$ . For any domain generalization transformation function  $g: \mathbb{D}_{\text{specific}} \rightarrow \mathbb{D}_{\text{common}}$ , such that  $g(\mathcal{G}, \mathcal{X}) = (\hat{\mathcal{G}}, \hat{\mathcal{X}})$ , there exists a learnable prompt  $P$  that satisfies:*

$$\mathcal{F}_\Theta((\mathcal{G}, \mathcal{X}) + P) = \mathcal{F}_\Theta(g(\mathcal{G}, \mathcal{X})). \quad (29)$$

Theorem 1 implies that a learnable prompt  $P$  can theoretically induce the same model behavior as applying a domain-generalizing transformation function  $g$ . Specifically, if  $g$  can map domain-specific data  $(\mathcal{G}, \mathcal{X})$  into a common representation  $(\mathcal{G}^*, \mathcal{X}^*)$  that enables effective learning, then optimizing the prompt  $P$  can likewise enable the model to produce equivalent generalizable outputs. To further illustrate the domain-generalized transformation  $g(\cdot)$  into spatio-temporal scenario, we decompose it into three specific sub-transformations.

**Proposition 1.** *Given the input spatio-temporal data  $(\mathcal{G}, \mathcal{X})$ , we extract the spatial scanned sequences  $\mathbf{S}$ , temporal scanned sequences  $\mathbf{X}$ , and ST-delay scanned sequences  $\mathbf{D}$ . Any domain-generalizing transformation function  $g: \mathbb{D}_{\text{specific}} \rightarrow \mathbb{D}_{\text{common}}$  can be decoupled into the composition of the following sub-transformations:*

- **Spatial pattern transformation:** Modifies the spatial node to obtain the generalized spatial representation  $\hat{\mathbf{S}} = g_S(\mathbf{S})$ .
- **Temporal pattern transformation:** Modifies the temporal features to obtain the generalized temporal representation  $\hat{\mathbf{X}} = g_T(\mathbf{X})$ .
- **ST-delay pattern transformation:** Modifies the delay-aware features to obtain the generalized spatio-temporal representation  $\hat{\mathbf{D}} = g_D(\mathbf{D})$ .

*Proof.* Please refer to Section A of the Supplementary Materials<sup>2</sup> for the complete proof.

<sup>2</sup><https://github.com/RuiAN77/Damba-ST>

## IV. EXPERIMENTS

In this section, we investigate the following key research questions to evaluate the effectiveness and efficiency of Damba-ST:

- **RQ1:** How does the Damba-ST perform in the In-distribution setting compared to existing spatio-temporal baselines?
- **RQ2:** What advantages does our proposed Damba-ST offer over baselines in cross-domain transfer learning?
- **RQ3:** What are the individual contributions of the different modules to the performance gains of the Damba-ST?
- **RQ4:** Compared to existing spatio-temporal foundation models, what advantages does Damba-ST have in terms of computational efficiency and deployment practicality?
- **RQ5:** How do different hyperparameter values affect the performance of Damba-ST?

### A. Experimental Setup

1) **Datasets:** In contrast to the region-specific, small-scale spatio-temporal datasets commonly used in prior studies, we conducted training and evaluation on large-scale public real-world datasets collected from multiple cities, including New York, Los Angeles, Shanghai, Shenzhen, and others [13]. These datasets span a variety of traffic-related domains, such as traffic flow, taxi demand, bicycle trajectories, and traffic speed. The pre-training dataset covers 10,110 regions and 352,796 time points, totaling 151,089,924 spatio-temporal observations [13]. These datasets vary in the number of variables, sampling frequency, spatial scale, temporal duration, and overall data volume. In the testing phase, we evaluated the model on datasets excluded from training, enabling an assessment of its generalization capability across diverse traffic prediction scenarios. Further details regarding the experimental datasets are provided in Section B of the Supplementary Materials.

2) **Baseline:** We have carefully selected the latest and advanced models in spatio-temporal prediction community as our baselines, which including: (1) Recent Spatio-Temporal foundation models: OpenCity [13], UniST [12]; (2) Mamba-based models: SpoT-Mamba [36], STG-Mamba [37]; (3) Attention-Based models: ASTGCN [38], STWA [6], PDFFormer [39]; and (4) GNNs-based models: STGCN [40], TGCN [41], GWN [8], MTGNN [42], STGCN [43].

3) **Metrics and Implementation Details:** We adopt widely used regression metrics to evaluate model performance: Mean Absolute Error (MAE), Root Mean Square Error (RMSE), and Mean Absolute Percentage Error (MAPE), where lower values indicate better performance. To ensure fair and comprehensive comparisons, we follow the experimental setup of [13]. All training and testing are conducted on a server equipped with 6x NVIDIA GeForce RTX A6000 48GB GPUs. Our largest model contains 12M parameters. For the long-term traffic forecasting task, we set both the historical and future time spans to 288 time steps. The patch length and stride are set to 12. The regularization weights are fixed across all datasets as  $\alpha = 1$  and  $\beta = 0.5$ , while the fusion weights are set to  $w_1 = 0.4$  and  $w_2 = 0.6$  during training. For all baselines, we adopt

the hyperparameter configurations as reported in their original papers or officially released implementations. Note that UniST is designed specifically for grid-based data and, therefore, does not produce results on graph-based datasets.

### B. In-distribution Prediction (RQ1)

1) **Setups:** We evaluate the adaptability of our proposed Damba-ST in an in-distribution scenario, where a large portion of the data is used for training, and the test set is held out for evaluation. Following the setup in [13], we assess the performance of the compared models in a long-term prediction setting. This is a challenging task due to the evolving temporal distribution shifts over longer time horizons. We directly use the pre-trained models of Damba-ST and OpenCity for testing, while other domain-specific baselines are trained end-to-end on their respective datasets.

2) **Results:** As shown in Table I, the results indicate that our proposed Damba-ST consistently outperforms the baselines across most evaluation metrics. Notably, we observed that almost all specialized models underperformed in the long-term traffic flow prediction task (i.e., on datasets CAD12-2, CAD8-2, and CAD8-1). This underperformance can primarily be attributed to these models' tendency to overfit historical spatio-temporal patterns, limiting their ability to generalize to future temporal shifts. In contrast, our proposed Damba-ST and OpenCity—both foundation models trained on large-scale datasets—have learned universal spatio-temporal knowledge from diverse data sources and exhibit robust generalization capabilities in this challenging task.

### C. Zero-shot Prediction (RQ2)

1) **Setups:** We conduct an out-of-distribution evaluation on unseen target datasets. In this context, Damba-ST serves as a zero-shot forecaster, compared with state-of-the-art full-shot baselines that have been trained on the individual target datasets. We assess the zero-shot generalization capability of Damba-ST across three different levels of difficulty in the zero-shot setting: (1) Cross-Region, which refers to testing on unseen geographical regions; (2) Cross-City, which involves testing in a new city; and (3) Cross-Task, which denotes testing on previously unseen types of traffic metrics.

2) **Results:** As shown in Table II, Damba-ST consistently ranks among the top two across multiple performance metrics, demonstrating its robustness even without fine-tuning on target domain data. This highlights the model's ability to learn complex spatio-temporal patterns from large-scale traffic data and extract universal insights applicable across unseen regions, different city patterns and unseen traffic tasks. A key advantage is its zero-retraining requirement, saving time and resources compared to traditional supervised methods. GWN demonstrates superior performance on CAD5 and PEMS07M compared to Damba-ST. This can be attributed to the fact that GWN has been specifically trained on these individual datasets, allowing it to perform exceptionally well as a specialized model, and it tends to struggle with other tasks. In contrast, Damba-ST is evaluated as a zero-shot forecaster on unseen target datasets and demonstrates consistent and strong performance across all

TABLE I: Results of in-distribution long-term prediction. The best results are highlighted in **red**, and the second-best results in **underlining**.

Dataset	Metrics	Foundation Model			Mamba-based models			Attention-based models			GNNs-based models			
		Damba-ST (Ours)	UniST [12]	OpenCity [13]	STG-Mamba [37]	SpoT-Mamba [36]	PDFormer [39]	STWA [6]	ASTGCN [38]	STGCN [43]	MTGNN [42]	GWN [8]	TGCN [41]	STGCN [40]
NYC-TAXI	MAE	<b>2.89</b>	3.52	<u>3.10</u>	4.56	4.13	3.64	6.05	5.45	5.03	3.72	4.28	6.10	4.17
	RMSE	<b>6.23</b>	8.60	<u>6.45</u>	11.46	9.26	8.24	15.22	13.44	10.96	7.94	10.59	12.70	9.19
	MAPE	<b>36.52%</b>	38.29%	<u>37.39%</u>	49.92%	39.42%	37.40%	54.81%	59.05%	65.17%	43.35%	41.82%	80.39%	45.54%
PEMS-BAY	MAE	<u>2.63</u>	-	<b>2.59</b>	2.80	2.77	2.75	2.74	2.82	2.87	2.59	2.66	2.94	2.72
	RMSE	5.71	-	<u>5.67</u>	6.42	6.82	6.15	5.65	6.31	6.10	5.43	<b>5.60</b>	6.33	5.96
	MAPE	5.97%	-	5.99%	7.28%	6.23%	6.50%	6.03%	7.06%	6.80%	<u>5.87%</u>	<b>5.94%</b>	7.23%	6.55%
CAD12-2	MAE	<b>22.37</b>	-	<u>24.20</u>	36.72	38.22	34.23	41.21	35.19	37.00	36.20	38.05	36.53	34.60
	RMSE	<b>37.32</b>	-	<u>39.23</u>	59.33	70.13	59.70	77.78	57.87	63.19	65.55	69.89	60.01	62.47
	MAPE	<b>32.58%</b>	-	<u>33.22%</u>	64.91%	66.34%	50.92%	67.72%	59.73%	58.29%	56.86%	64.77%	61.60%	52.49%
CAD8-2	MAE	<u>18.35</u>	-	<b>17.95</b>	25.91	26.12	24.32	26.57	24.24	24.60	21.85	25.17	23.43	24.30
	RMSE	<b>29.35</b>	-	<u>29.61</u>	39.73	42.77	38.95	44.01	38.14	41.23	34.02	41.47	37.03	39.59
	MAPE	<u>12.32%</u>	-	<b>10.97%</b>	19.28%	19.27%	14.84%	20.21%	18.36%	18.54%	14.20%	18.50%	15.55%	18.61%
CAD8-1	MAE	<b>21.59</b>	-	<u>22.50</u>	30.22	30.56	29.64	32.09	29.38	32.38	31.60	29.03	27.68	31.26
	RMSE	<b>38.35</b>	-	<u>39.06</u>	49.98	51.34	49.79	32.09	46.84	53.28	53.01	49.26	45.09	49.91
	MAPE	<b>15.52%</b>	-	<u>15.50%</u>	24.38%	24.56%	20.65%	25.62%	22.51%	25.63%	25.82%	23.23%	20.18%	24.26%
1 <sup>st</sup> Count		<b>9</b>	0	<u>4</u>	0	0	0	0	0	0	0	2	0	0

TABLE II: Results of Zero-shot Prediction. Performance comparison between Damba-ST under the zero-shot setting and baseline models under the full-shot setting across three increasingly challenging cross-domain tasks: Cross-Region, Cross-City, and Cross-Task.

Dataset	Metrics	Foundation Model			Mamba-based Models			Attention-based Models			GNNs-based Models			
		Damba-ST (Ours)	UniST [12]	OpenCity [13]	STGMamba [37]	SpoTMamba [36]	PDFormer [39]	STWA [6]	ASTGCN [38]	STGCN [43]	MTGNN [42]	GWN [8]	TGCN [41]	STGCN [40]
Region	MAE	<b>14.21</b>	-	<u>15.88</u>	21.35	22.73	20.28	21.65	23.60	21.88	17.59	16.94	19.56	20.24
	RMSE	<b>24.75</b>	-	<u>27.03</u>	36.92	37.12	36.43	37.55	39.35	34.52	28.92	28.81	30.82	34.34
	MAPE	<b>20.03%</b>	-	<u>21.94%</u>	25.97%	26.93%	25.19%	26.85%	41.22%	30.20%	25.22%	22.98%	28.15%	25.33%
CAD5	MAE	<u>10.77</u>	-	11.09	12.94	13.27	12.89	14.43	12.58	13.87	11.70	<b>10.69</b>	13.07	13.76
	RMSE	<b>18.27</b>	-	<u>18.96</u>	23.52	23.12	21.18	24.14	21.23	22.32	20.30	19.75	21.56	27.49
	MAPE	<b>26.31%</b>	-	27.90%	30.06%	29.77%	28.82%	29.34%	30.56%	32.84%	26.75%	<b>25.98%</b>	32.65%	32.89%
PEMS07M	MAE	4.53	-	4.50	4.65	4.77	4.62	4.54	<u>4.39</u>	4.56	4.52	<b>4.17</b>	4.88	4.44
	RMSE	8.33	-	8.21	8.92	8.43	8.36	8.57	8.21	<u>8.05</u>	8.06	<b>7.84</b>	8.38	8.37
	MAPE	12.57%	-	<u>12.20%</u>	13.28%	14.02%	13.74%	12.91%	12.58%	12.70%	13.11%	<b>11.46%</b>	13.94%	12.59%
TrafficSH	MAE	<b>0.51</b>	1.26	<u>0.55</u>	1.24	1.13	0.77	1.42	0.69	1.66	0.81	0.76	1.79	1.60
	RMSE	<b>0.85</b>	1.72	<u>0.85</u>	2.83	2.97	1.23	2.49	1.09	3.33	1.26	1.39	2.65	3.14
	MAPE	<b>7.83%</b>	8.69%	<u>8.01%</u>	10.03%	10.39%	8.34%	9.92%	8.05%	9.33%	8.29%	9.23%	17.75%	8.04%
CHI-TAXI	MAE	<u>2.05</u>	4.26	<b>1.91</b>	3.88	4.25	4.03	3.70	3.28	4.87	3.27	3.56	4.02	3.09
	RMSE	<u>4.53</u>	13.57	<b>4.42</b>	11.32	13.94	12.82	11.49	10.32	14.40	9.87	11.27	11.70	9.54
	MAPE	42.31%	45.29%	<u>40.07%</u>	45.73%	46.72%	44.42%	42.52%	42.82%	104.64%	<b>39.38%</b>	41.31%	60.25%	42.47%
Task	MAE	<b>6.09</b>	7.36	<u>6.32</u>	6.94	7.23	7.33	7.97	6.44	6.85	6.48	7.61	7.75	8.01
	RMSE	<b>11.46</b>	12.58	11.60	12.95	13.46	13.01	14.35	11.62	11.98	<u>11.49</u>	13.56	13.49	13.94
	MAPE	<b>60.27%</b>	65.39%	70.06%	64.76%	63.29%	65.44%	64.19%	63.90%	68.44%	61.52%	<b>58.41%</b>	85.27%	63.02%
1 <sup>st</sup> Count		<b>9</b>	0	<u>3</u>	0	0	0	0	0	0	1	6	0	0

tested datasets, showcasing its versatility as a general-purpose model.

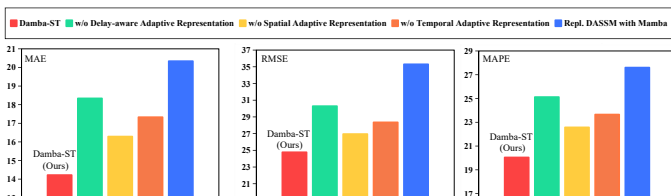


Fig. 3: Ablation Study on Damba-ST.

#### D. Ablation Study (RQ3)

To validate the effectiveness of the key components in Damba-ST, we conducted an ablation study under zero-shot

settings using the CAD3 dataset. The ablation study includes the following variants: replacing (*Repl.*) the DASSM module with vanilla Mamba in three DASSM variants, and individually removing the DASSM<sub>S</sub>, the DASSM<sub>T</sub>, and the DASSM<sub>D</sub>. As shown in Fig. 3, we can make the following observations:

- **Repl. DASSM:** When replacing DASSM with Mamba, the model reverts to fusion training and fails to capture the heterogeneity of the data. This results in the most significant performance degradation, as the model loses its ability to learn domain-adaptive representations.
- **w/o DASSM<sub>S</sub> (Spatial View):** Removing the Spatial Adaptive Representation leads to a noticeable increase in error metrics. By considering the structural information of the traffic graph, the model can capture generalized spatial-

topology-related traffic patterns, which are crucial for cross-region generalization.

- **w/o DASSM<sub>T</sub> (Temporal View):** Removing the Temporal Adaptive Representation results in a significant degradation of performance, as the temporal view provides essential information about the series’s own dynamics. This allows the model to capture time-dependent traffic patterns, which are crucial for making accurate predictions in evolving traffic conditions.
- **w/o DASSM<sub>D</sub> (ST-delay View):** Removing the Delay-Aware Adaptive Representation causes a significant performance drop. The ST-delay View provides knowledge of spatio-temporal delay dependencies, which is crucial for real-world traffic prediction, as it captures the delayed interactions between spatial and temporal factors.

#### E. Efficiency Analysis and Deployment Practicality (RQ4)

Damba-ST theoretically offers significant advantages over Transformer-based spatio-temporal foundation models in terms of training complexity, inference complexity, and memory usage, as shown in Table III. Specifically, the computational complexity of Damba-ST scales linearly with the input sequence length  $L$ , whereas Transformer-based models typically exhibit quadratic complexity with respect to  $L$ . This makes Damba-ST more efficient and memory-friendly. We empirically validate these advantages on real-world datasets from *Training Efficiency* and *Deployment Practicality*.

TABLE III: Complexity Analysis and Deployment Practicality.  $L$  is input sequence length,  $D$  is the hidden dimension,  $L \gg D$ .

Comparison	Transformer-based		Mamba-based
	UniST [12]	OpenCity [13]	Damba-ST(Ours)
Training Complexity	$\mathcal{O}(L^2D)$	$\mathcal{O}(L^2D)$	$\mathcal{O}(3LD^2)$
Inference Complexity	$\mathcal{O}(LD)$	$\mathcal{O}(LD)$	$\mathcal{O}(3D^2)$
Memory	$\mathcal{O}(L^2)$	$\mathcal{O}(L^2)$	$\mathcal{O}(3LD)$
MAE	2.94	1.74	1.51
RMSE	7.88	3.80	3.22
Cost (seconds)	1.3s	1.5s	0.9s

1) **Training Efficiency:** As shown in Fig. 4, we compare the proposed Damba-ST against existing spatio-temporal foundation models UniSA [12] and OpenCity [13] in terms of Running Time (i.e., Training Speed) and GPU memory usage for long-term forecasting tasks, where the lookback window length increases quadratically from {384, 768, 1536, 3072}. The figure demonstrates that transformer-based spatiotemporal foundation models, i.e., UniSA and OpenCity, suffer from quadratic complexity, resulting in high memory usage and slower training speeds. In contrast, the Mamba-based Damba-ST offers a more efficient trade-off between performance, training speed, and memory usage. Damba-ST consistently shows superior efficiency in both training time and GPU memory usage across varying series lengths, achieving a favorable balance between performance and computational cost.

2) **Deployment Practicality:** Given that all experimental datasets are sourced from real-world urban environments, we

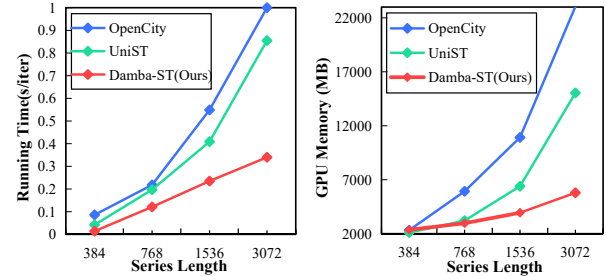


Fig. 4: Efficiency analysis of running time and GPU memory in long-term prediction. Damba-ST scales linearly with the series length.

further evaluate the practical efficiency of Damba-ST under deployment settings. To simulate a realistic application scenario, we test Damba-ST on the CHI-TAXI dataset—which was not included during pre-training—by performing next-day traffic prediction using the previous day’s data. The model is deployed on an NVIDIA GeForce RTX A6000 48GB GPU.

As shown in Table III, Damba-ST not only achieves the best predictive performance in terms of MSE and RMSE but also demonstrates remarkable inference efficiency, completing each prediction in just 0.9 seconds. This rapid response time underscores Damba-ST’s suitability for real-time urban applications and highlights its potential as a robust and deployable spatio-temporal foundation model—offering a win-win solution in both prediction accuracy and computational efficiency.

#### F. Hyperparameter Sensitivity Analysis (RQ5)

We evaluate the hyperparameter sensitivity of Damba-ST on three zero-shot datasets. Specifically, we examine two sets of hyperparameters: (1) the fusion weights  $w_1$  and  $w_2$ , which control the trade-off between the Discriminative Representation and Common Representation in the DASSM fusion layer (as shown in Eq (19)); and (2) the regularization weights  $\alpha$  and  $\beta$ , which govern the similarity constraint term in the objective function (as shown in Eq (26)). The evaluation metric is MAE.

As shown in Fig. 5(a)-(c), we perform grid searches over fusion weights  $w_1, w_2 \in \{0.2, 0.4, 0.6, 0.8\}$ . We find that the fusion weights  $w_1$  and  $w_2$  should be carefully selected based on the differences between the training and testing data. Specifically, when testing on an unseen region, assigning a higher weight to the Discriminative Representation weights  $w_1$  typically yields better results (as shown in Fig. 5(a)). Conversely, when testing on an unseen task—which is more challenging than a cross-region task—the model’s overall generalization capability becomes crucial, and thus, a higher weight on the Common Representation weights  $w_2 = 0.8$  tends to produce superior performance (as shown in Fig. 5(b)).

As shown in Fig. 5 (d)-(f), We perform grid searches of  $\alpha, \beta \in \{0, 0.2, 0.5, 1, 5\}$ . We find that increasing  $\alpha, \beta$  generally improves performance, with the best results at  $\alpha = 1, \beta = 0.5$ . Beyond this point, the performance stabilizes or slightly decreases, indicating that while regularization is crucial, excessive regularization can slightly reduce the performance.

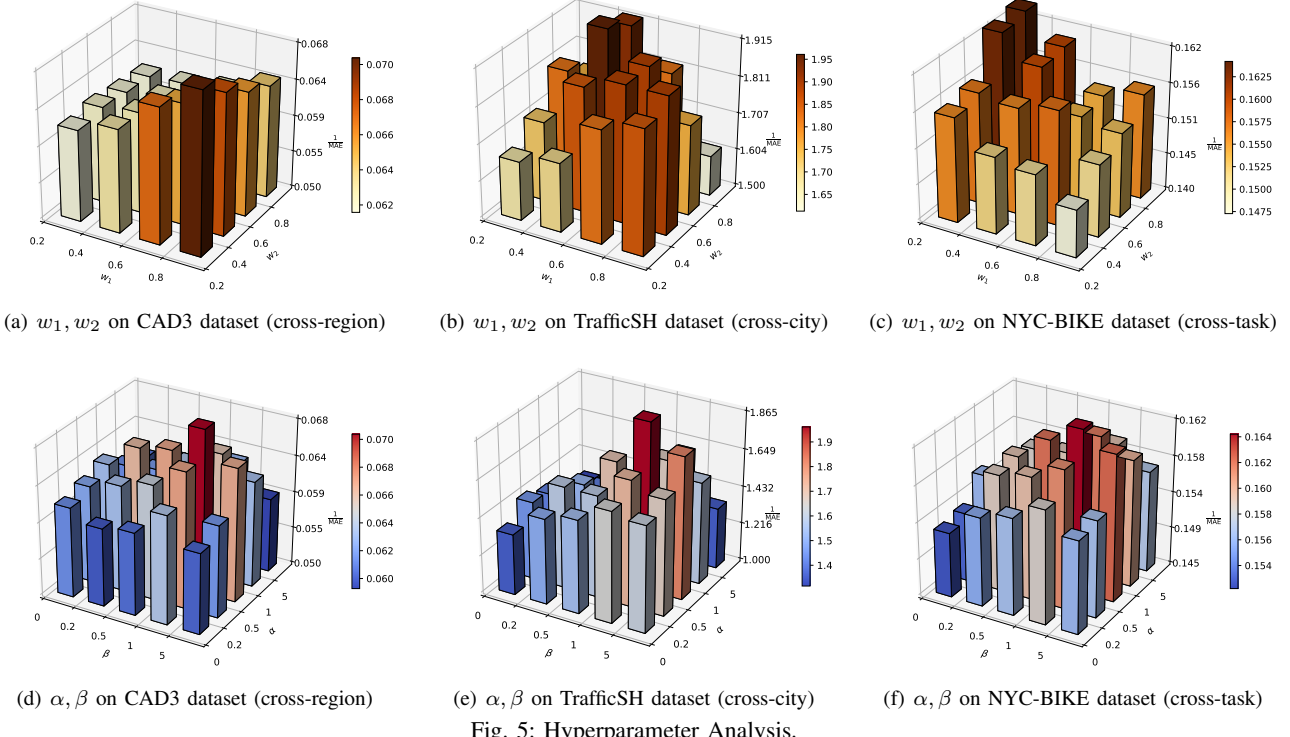


Fig. 5: Hyperparameter Analysis.

## V. RELATED WORK

### A. Spatio-temporal Foundation Models.

Inspired by the significant advancements in foundation models for NLP and CV, a notable line of work has explored Spatio-temporal Foundation Models. Some LLM-based models, such as CityGPT [44], CityBench [45], and UrbanGPT [46], have demonstrated proficiency in addressing language-based urban tasks. LLMs have been employed to generate descriptions of urban-related images, thus aiding downstream tasks such as urban scene understanding [44]. While the integration of LLMs into urban systems shows great promise, it is important to recognize that spatio-temporal data is not inherently generated by language; the modality gap limits the direct application of LLMs to spatio-temporal tasks. Recent efforts have focused on training spatio-temporal foundation models from scratch. For instance, UniST [12] was developed for grid-based urban scenarios, allowing it to generalize to new situations without additional training. Similarly, OpenCity [13] integrates the Transformer architecture with graph neural networks to model complex spatio-temporal dependencies, benefiting from pretraining on large-scale data. Despite these advancements, the high computational requirements of the Transformer architecture pose challenges for computational efficiency and real-world deployment. Moreover, the fusion training methods induce challenges in generalization due to spatio-temporal heterogeneity. Consequently, there is an urgent need to develop more efficient and generalized models that can effectively capture universal spatio-temporal patterns across diverse, heterogeneous spatio-temporal scenarios.

### B. *Mamba-based Spatio-Temporal Model*.

Inspired by the superior performance of Mamba models across various domains [16], including language modeling [18], speech analysis [47], and recommender systems [48], researchers have recently started exploring the applicability of Mamba for spatio-temporal forecasting and spatial-temporal graph learning [36], [37], [49], [50]. For instance, STG-Mamba [37] treats the spatio-temporal graph evolution process as a system and employs a selective mechanism to focus on relevant latent features. SpOT-Mamba [36] performs Mamba scanning across both spatial and temporal dimensions to capture corresponding dependencies. ST-Mamba integrates CNNs with Mamba for traffic flow estimation. While these models leverage Mamba's computational efficiency and strong performance for specific tasks and domains, to date, no research has explored Mamba as a spatio-temporal foundation model capable of generalizing across diverse urban scenarios.

## VI. CONCLUSION

Training urban spatio-temporal models that generalize across cities is challenging due to data heterogeneity and computational complexity. To tackle these issues, we introduce Damba-ST, which addresses spatio-temporal heterogeneity through domain adapters, three scan strategies, and a domain-adaptive selective state space model to capture both shared and domain-specific features. Our experiments demonstrate that Damba-ST achieves state-of-the-art performance, with superior zero-shot capabilities, enabling seamless deployment in new environments without retraining.

## REFERENCES

[1] Y. Zheng, L. Capra, O. Wolfson, and H. Yang, "Urban computing: concepts, methodologies, and applications," *ACM Transactions on Intelligent Systems and Technology (TIST)*, vol. 5, no. 3, pp. 1–55, 2014.

[2] H. Xia, X. Zhang, Y. Cao, L. Cao, Y. Yu, and J. Dong, "Self-supervised trajectory representation learning with multi-scale spatio-temporal feature exploration," in *2025 IEEE 41st International Conference on Data Engineering (ICDE)*. Los Alamitos, CA, USA: IEEE Computer Society, May 2025, pp. 779–792. [Online]. Available: <https://doi.ieeecomputersociety.org/10.1109/ICDE65448.2025.00064>

[3] M. Jin, Q. Wen, Y. Liang, C. Zhang, S. Xue, X. Wang, J. Zhang, Y. Wang, H. Chen, X. Li *et al.*, "Large models for time series and spatio-temporal data: A survey and outlook," *arXiv preprint arXiv:2310.10196*, 2023.

[4] B. Yang, Y. Liang, C. Guo, and C. S. Jensen, "Data driven decision making with time series and spatio-temporal data," in *2025 IEEE 41st International Conference on Data Engineering (ICDE)*. Los Alamitos, CA, USA: IEEE Computer Society, May 2025, pp. 4517–4522. [Online]. Available: <https://doi.ieeecomputersociety.org/10.1109/ICDE65448.2025.00343>

[5] P. Xie, T. Li, J. Liu, S. Du, X. Yang, and J. Zhang, "Urban flow prediction from spatiotemporal data using machine learning: A survey," *Information Fusion*, vol. 59, pp. 1–12, 2020.

[6] R.-G. Cirstea, B. Yang, C. Guo, T. Kieu, and S. Pan, "Towards spatio-temporal aware traffic time series forecasting," in *2022 IEEE 38th International Conference on Data Engineering (ICDE)*. IEEE, 2022, pp. 2900–2913.

[7] R. Li, H. He, R. Wang, Y. Huang, J. Liu, S. Ruan, T. He, J. Bao, and Y. Zheng, "Just: Jd urban spatio-temporal data engine," in *2020 IEEE 36th International Conference on Data Engineering (ICDE)*, 2020, pp. 1558–1569.

[8] Z. Wu, S. Pan, G. Long, J. Jiang, and C. Zhang, "Graph wavenet for deep spatial-temporal graph modeling," *arXiv preprint arXiv:1906.00121*, 2019.

[9] R. Yu, Y. Li, C. Shahabi, U. Demiryurek, and Y. Liu, "Deep learning: A generic approach for extreme condition traffic forecasting," in *Proceedings of the 2017 SIAM international Conference on Data Mining*. SIAM, 2017, pp. 777–785.

[10] C. Zheng, X. Fan, C. Wang, and J. Qi, "Gman: A graph multi-attention network for traffic prediction," in *Proceedings of the AAAI conference on artificial intelligence*, vol. 34, no. 01, 2020, pp. 1234–1241.

[11] Q. Luo, S. He, X. Han, Y. Wang, and H. Li, "Lsttn: A long-short term transformer-based spatiotemporal neural network for traffic flow forecasting," *Knowledge-Based Systems*, vol. 293, p. 111637, 2024.

[12] Y. Yuan, J. Ding, J. Feng, D. Jin, and Y. Li, "Unist: A prompt-empowered universal model for urban spatio-temporal prediction," in *Proceedings of the 30th ACM SIGKDD Conference on Knowledge Discovery and Data Mining*, 2024, pp. 4095–4106.

[13] Z. Li, L. Xia, L. Shi, Y. Xu, D. Yin, and C. Huang, "Opencity: Open spatio-temporal foundation models for traffic prediction," *arXiv preprint arXiv:2408.10269*, 2024.

[14] Y. Fang, Y. Qin, H. Luo, F. Zhao, B. Xu, L. Zeng, and C. Wang, "When spatio-temporal meet wavelets: Disentangled traffic forecasting via efficient spectral graph attention networks," in *2023 IEEE 39th International Conference on Data Engineering (ICDE)*. IEEE, 2023, pp. 517–529.

[15] A. Gu and T. Dao, "Mamba: Linear-time sequence modeling with selective state spaces," *arXiv preprint arXiv:2312.00752*, 2023.

[16] H. Qu, L. Ning, R. An, W. Fan, T. Derr, X. Xu, and Q. Li, "A survey of mamba," *arXiv preprint arXiv:2408.01129*, 2024.

[17] T. Dao and A. Gu, "Transformers are ssms: Generalized models and efficient algorithms through structured state space duality," *arXiv preprint arXiv:2405.21060*, 2024.

[18] O. Lieber, B. Lenz, H. Bata, G. Cohen, J. Osin, I. Dalmedigos, E. Safahi, S. Meirom, Y. Belinkov, S. Shalev-Shwartz *et al.*, "Jamba: A hybrid transformer-mamba language model," *arXiv preprint arXiv:2403.19887*, 2024.

[19] L. Zhu, B. Liao, Q. Zhang, X. Wang, W. Liu, and X. Wang, "Vision mamba: Efficient visual representation learning with bidirectional state space model," *arXiv preprint arXiv:2401.09417*, 2024.

[20] K. Li, X. Li, Y. Wang, Y. He, Y. Wang, L. Wang, and Y. Qiao, "Videomamba: State space model for efficient video understanding," in *European Conference on Computer Vision*. Springer, 2025, pp. 237–255.

[21] Y. Schiff, C.-H. Kao, A. Gokaslan, T. Dao, A. Gu, and V. Kuleshov, "Caduceus: Bi-directional equivariant long-range dna sequence modeling," *arXiv preprint arXiv:2403.03234*, 2024.

[22] S. Long, Q. Zhou, X. Li, X. Lu, C. Ying, Y. Luo, L. Ma, and S. Yan, "Dgmamba: Domain generalization via generalized state space model," in *Proceedings of the 32nd ACM International Conference on Multimedia*, 2024, pp. 3607–3616.

[23] A. Gu, T. Dao, S. Ermon, A. Rudra, and C. Ré, "Hippo: Recurrent memory with optimal polynomial projections," *Advances in neural information processing systems*, vol. 33, pp. 1474–1487, 2020.

[24] M. Harris, S. Sengupta, and J. D. Owens, "Parallel prefix sum (scan) with cuda," *GPU gems*, vol. 3, no. 39, pp. 851–876, 2007.

[25] A. Dosovitskiy, L. Beyer, A. Kolesnikov, D. Weissenborn, X. Zhai, T. Unterthiner, M. Dehghani, M. Minderer, G. Heigold, S. Gelly *et al.*, "An image is worth 16x16 words: Transformers for image recognition at scale," *ICLR*, 2021.

[26] Y. Zou, S. Yi, Y. Li, and R. Li, "A closer look at the cls token for cross-domain few-shot learning," *Advances in Neural Information Processing Systems*, vol. 37, pp. 85 523–85 545, 2024.

[27] T. Dariseti, M. Oquab, J. Mairal, and P. Bojanowski, "Vision transformers need registers," *arXiv preprint arXiv:2309.16588*, 2023.

[28] T. Kim, J. Kim, Y. Tae, C. Park, J.-H. Choi, and J. Choo, "Reversible instance normalization for accurate time-series forecasting against distribution shift," in *International Conference on Learning Representations*, 2021.

[29] Y. Nie, N. H. Nguyen, P. Sinthong, and J. Kalagnanam, "A time series is worth 64 words: Long-term forecasting with transformers," in *The Eleventh International Conference on Learning Representations*, 2023.

[30] M. Azaria and D. Hertz, "Time delay estimation by generalized cross correlation methods," *IEEE Transactions on Acoustics, Speech, and Signal Processing*, vol. 32, no. 2, pp. 280–285, 1984.

[31] Q. Long, Z. Fang, C. Fang, C. Chen, P. Wang, and Y. Zhou, "Unveiling delay effects in traffic forecasting: A perspective from spatial-temporal delay differential equations," in *Proceedings of the ACM on Web Conference 2024*, 2024, pp. 1035–1044.

[32] Z. Zhang, W. Jiang, J. Qin, L. Zhang, F. Li, M. Zhang, and S. Yan, "Jointly learning structured analysis discriminative dictionary and analysis multiclass classifier," *IEEE transactions on neural networks and learning systems*, vol. 29, no. 8, pp. 3798–3814, 2017.

[33] Y. Zhang, Y. Wang, Y. Li, Y. Xu, S. Wei, S. Liu, and X. Shang, "Federated discriminative representation learning for image classification," *IEEE Transactions on Neural Networks and Learning Systems*, 2023.

[34] T. Fang, Y. Zhang, Y. Yang, C. Wang, and L. Chen, "Universal prompt tuning for graph neural networks," *Advances in Neural Information Processing Systems*, vol. 36, pp. 52 464–52 489, 2023.

[35] H. Zhao, A. Chen, X. Sun, H. Cheng, and J. Li, "All in one and one for all: A simple yet effective method towards cross-domain graph pretraining," in *Proceedings of the 30th ACM SIGKDD Conference on Knowledge Discovery and Data Mining*, 2024, pp. 4443–4454.

[36] J. Choi, H. Kim, M. An, and J. J. Whang, "Spot-mamba: Learning long-range dependency on spatio-temporal graphs with selective state spaces," *arXiv preprint arXiv:2406.11244*, 2024.

[37] L. Li, H. Wang, W. Zhang, and A. Coster, "Stg-mamba: Spatial-temporal graph learning via selective state space model," *arXiv preprint arXiv:2403.12418*, 2024.

[38] S. Guo, Y. Lin, N. Feng, C. Song, and H. Wan, "Attention based spatial-temporal graph convolutional networks for traffic flow forecasting," in *Proceedings of the AAAI conference on artificial intelligence*, vol. 33, no. 01, 2019, pp. 922–929.

[39] J. Jiang, C. Han, W. X. Zhao, and J. Wang, "Pdformer: Propagation delay-aware dynamic long-range transformer for traffic flow prediction," in *Proceedings of the AAAI conference on artificial intelligence*, vol. 37, no. 4, 2023, pp. 4365–4373.

[40] B. Yu, H. Yin, and Z. Zhu, "Spatio-temporal graph convolutional networks: A deep learning framework for traffic forecasting," in *Proceedings of the 27th International Joint Conference on Artificial Intelligence (IJCAI)*, 2018.

[41] L. Zhao, Y. Song, C. Zhang, Y. Liu, P. Wang, T. Lin, M. Deng, and H. Li, "T-gcn: A temporal graph convolutional network for traffic prediction," *IEEE transactions on intelligent transportation systems*, vol. 21, no. 9, pp. 3848–3858, 2019.

[42] Z. Wu, S. Pan, G. Long, J. Jiang, X. Chang, and C. Zhang, "Connecting the dots: Multivariate time series forecasting with graph neural networks," in *Proceedings of the 26th ACM SIGKDD international conference on knowledge discovery & data mining*, 2020, pp. 753–763.

- [43] C. Song, Y. Lin, S. Guo, and H. Wan, “Spatial-temporal synchronous graph convolutional networks: A new framework for spatial-temporal network data forecasting,” in *Proceedings of the AAAI conference on artificial intelligence*, vol. 34, no. 01, 2020, pp. 914–921.
- [44] J. Feng, Y. Du, T. Liu, S. Guo, Y. Lin, and Y. Li, “Citygpt: Empowering urban spatial cognition of large language models,” *arXiv preprint arXiv:2406.13948*, 2024.
- [45] J. Feng, J. Zhang, J. Yan, X. Zhang, T. Ouyang, T. Liu, Y. Du, S. Guo, and Y. Li, “Citybench: Evaluating the capabilities of large language model as world model,” *arXiv preprint arXiv:2406.13945*, 2024.
- [46] Z. Li, L. Xia, J. Tang, Y. Xu, L. Shi, L. Xia, D. Yin, and C. Huang, “Urbangpt: Spatio-temporal large language models,” in *Proceedings of the 30th ACM SIGKDD Conference on Knowledge Discovery and Data Mining*, 2024, pp. 5351–5362.
- [47] C. Quan and X. Li, “Multichannel long-term streaming neural speech enhancement for static and moving speakers,” *arXiv preprint arXiv:2403.07675*, 2024.
- [48] H. Qu, Y. Zhang, L. Ning, W. Fan, and Q. Li, “Ssd4rec: A structured state space duality model for efficient sequential recommendation,” *arXiv preprint arXiv:2409.01192*, 2024.
- [49] Z. Shao, M. G. Bell, Z. Wang, D. G. Geers, H. Xi, and J. Gao, “St-ssms: Spatial-temporal selective state of space model for traffic forecasting,” *arXiv preprint arXiv:2404.13257*, 2024.
- [50] D. Yuan, J. Xue, J. Su, W. Xu, and H. Zhou, “St-mamba: Spatial-temporal mamba for traffic flow estimation recovery using limited data,” in *2024 IEEE/CIC International Conference on Communications in China (ICCC)*. IEEE, 2024, pp. 1928–1933.